International Journal of Heat and Fluid Flow 57 (2016) 130–141

Contents lists available at ScienceDirect

International Journal of Heat and Fluid Flow

journal homepage: www.elsevier.com/locate/ijheatfluidflow

DNS study of a pipe flow following a step increase in flow rate

K. He [a], M. Seddighi [a,b], S. He [a,*]

[a] Department of Mechanical Engineering, University of Sheffield, Sheffield S1 3JD, UK
[b] Department of Maritime and Mechanical Engineering, Liverpool John Moores University, Liverpool L3 3AF, UK

ARTICLE INFO

Article history:
Received 11 June 2015
Revised 21 August 2015
Accepted 25 September 2015

Keywords:
Transient flow
Pipe flow
Flow acceleration
Bypass transition

ABSTRACT

Direct numerical simulation (DNS) is conducted to study the transient flow in a pipe following a near-step increase of flow rate from an initial turbulent flow. The results are compared with those of the transient flow in a channel reported in He and Seddighi (2013). It is shown that the flow again exhibits a laminar–turbulent transition, similar to that in a channel. The behaviours of the flow in a pipe and a channel are the same in the near-wall region, but there are significant differences in the centre of the flow. The correlation between the critical Reynolds number and free stream turbulence previously established for a channel flow has been shown to be applicable to the pipe flow. The responses of turbulent viscosity, vorticity Reynolds number, and budget terms are analysed. Some significant differences have been found to exist between the developments of the vorticity Reynolds number in the pipe and channel flows.

1. Introduction

Transient flows exist in many natural and engineering systems. Some of them are harmful and may lead to economical loses or safety concerns. A typical example is a pump on/off event or valve malfunction, which may potentially induce significant transients resulting in strong pressure waves travelling through a pipe network, potentially causing major damages to a civil water system (Colombo et al., 2009; Ghidaoui et al., 2005). A good understanding of transient flow not only helps in designing safer and more economical engineering systems, but is also useful in developing a better understanding of turbulent flow in general. The studies of turbulence during a transient process (He and Jackson, 2000; He and Seddighi, 2013, 2015; Seddighi et al., 2014) have revealed physical phenomena that are not obvious in steady flows, providing a strong incentive for further investigations.

Unsteady transient flows can typically be categorized into two groups, i.e. periodic (oscillating or pulsating) and non-periodic (acceleration/deceleration) flows. Whereas there is a large body of studies on the former (Mizushina et al., 1975; Akhavan et al., 1991; Choi et al., 1997; Maurizio and Stefano, 2000; He and Jackson, 2009) fewer studies have been performed on the latter (Kataoka et al., 1975; Maruyama et al., 1976; He and Jackson, 2000; Greenblatt and Moss, 2004; Seddighi et al., 2011). Step acceleration and deceleration flows have been investigated experimentally since the 1970s (Kataoka et al., 1975; Maruyama et al., 1976). An important finding was that in both flows, turbulence first responds near the wall and then propagates outwards. He and Jackson (2000) conducted a detailed experimental study of turbulent pipe flow with a constant temporal acceleration or deceleration. They identified important processes which were used to explain unsteady turbulence responses, namely, the response of turbulence production, turbulence energy redistribution among its three components, and the propagation of turbulence radially. Although a multitude of knowledge is gained through experiments, the understanding of the detailed flow structures and dynamics is still limited. Computational fluid dynamic (CFD) based on RANS (Reynolds-averaged Navier–Stokes) modelling has been used to complement the experiments to improve our understanding of the transient flow phenomena (e.g. Mankbadi and Liu, 1992; He et al., 2008). Even though some turbulences models can be used to reproduce many interesting flow behaviours with some success (Gorji et al., 2014), the RANS modelling, by virtue of its nature, has limited capability in offering new understanding of the physics. By contrast, direct numerical simulation (DNS) resolves all the detailed flow physics without using empirical models. Recently, based on DNS simulation of transient channel flow following a near-step increase in flow rate, He and Seddighi (2013) (referred to as HS2013 hereafter) proposed that the transient process is effectively a laminar–turbulent bypass transition even though the initial flow is turbulent. The transient process undergoes three distinct stages, namely, *pre-transition*, *transition*, and *fully-developed turbulent flow*.

The mechanisms of boundary layer bypass transition have been studied intensively (Jacobs and Durbin, 2001; Zaki and Durbin, 2005; Nagarajan et al., 2007; Schlatter et al., 2008). The process of the bypass transition can be divided into three regions, namely, a buffeted

* Corresponding author. Tel.: +44 114 222 7756.
E-mail address: s.he@sheffield.ac.uk (S. He).

http://dx.doi.org/10.1016/j.ijheatfluidflow.2015.09.004

laminar boundary layer, a region with isolated turbulent spots and a fully turbulent boundary layer. Large scale perturbations from the free-stream turbulence (FST) penetrate into the laminar boundary layer which is then amplified to produce elongated low- and high-speed streaks, remaining largely stable initially. Towards the end of this region, the flow reaches a condition such that secondary instability leads to turbulent spots, which evolve and grow, occupying increasingly more spaces until they fill the full span of the flow field and the flow subsequently becomes fully turbulent. Previous research (Jacobs and Durbin, 2001) shows that multiple factors affect the bypass transition, including the level, the disturbance spatial scales, the energy spectrum, the degree of isotropy and homogeneity of FST. It was suggested that the transient channel flow represents an alternative bypass transition scenario to the free-stream turbulence induced transition, whereby the disturbances are turbulence in a turbulent wall shear flow with pre-existing streaky structures (HS2013). Later, He and Seddighi (2015) studied the effect of varying the initial and final Reynolds numbers of the transient channel flow. It was shown that the onset of transition is a function of the initial free stream turbulence level, Tu_0, based on the initial turbulence and the final bulk velocity. It has been established through both theoretical and experimental investigations that for spatially developing boundary, $Re_{cr} \sim Tu_0^{-2}$ (Andersson et al., 1999; Brandt et al., 2004; Fransson et al., 2005; Ovchinnikov et al., 2008). Analogy to boundary layer flow, the onset of transition in transient channel flow has been found to be dependent on Tu_0 as $Re_{t,cr} \sim Tu_0^{-1.71}$, where $Re_{t,cr} = t_{cr}{}^* U_{b1}{}^2/\nu$ and $t_{cr}{}^*$ is the time of the transition onset (He and Seddighi, 2015).

The present paper extends previous DNS studies on the transient channel flow (HS2013; He and Seddighi, 2015) to investigate corresponding transient flow in a pipe. It has been established that channel and pipe flows are similar in the near wall region, but there are various differences between the two flows in the core of the flow field. Nagib and Chauhan (2008) studied the wake parameter based on a large data set with a wide range of Reynolds numbers and concluded that its value is higher in pipes than in channels. However, the origin of the difference between the channel and pipe is still unclear (Wosnik et al., 2000). Theoretical analysis of Meseguer and Trefethen (2003) shows that the pipe flow is linearly stable for all Reynolds numbers while the channel flow has a critical Reynolds number beyond which the flow is linearly unstable. Very recently, Chin (2011) showed that the pipe flow is dominated by small-scale structures in the core region, whereas the channel flow is dominated by large-scale motions. In this paper, we will compare the transient flows in a pipe and a channel and discuss the transition mechanisms in a transient flow.

2. Methodology

The channel flow DNS code of Seddighi (2011) has been modified to simulate the flow in a pipe. The dimensionless forms of the momentum and continuity equations are written as:

$$r\frac{\partial q_z}{\partial z} + \frac{\partial q_r}{\partial r} + \frac{1}{r}\frac{\partial q_\theta}{\partial \theta} = 0 \tag{1}$$

$$\frac{\partial q_z}{\partial t} + \frac{\partial q_z q_z}{\partial z} + \frac{1}{r}\frac{\partial q_r q_z}{\partial r} + \frac{1}{r^2}\frac{\partial q_r \theta q_z}{\partial \theta} = -\frac{\partial p}{\partial z} - \frac{\partial \overline{P}}{\partial z} + \frac{1}{Re_p}\left(\frac{\partial^2 q_z}{\partial z^2} + \frac{1}{r}\frac{\partial}{\partial r}r\frac{\partial q_z}{\partial r} + \frac{1}{r^2}\frac{\partial^2 q_z}{\partial \theta^2}\right) \tag{2}$$

$$\frac{\partial q_r}{\partial t} + \frac{\partial q_r q_z}{\partial z} + \frac{\partial q_r (q_r/r)}{\partial r} + \frac{\partial (q_\theta q_r)/r^2}{\partial \theta} - \frac{{q_\theta}^2}{r^2} = -r\frac{\partial p}{\partial r} + \frac{1}{Re_p}\left(\frac{\partial^2 q_r}{\partial z^2} + \frac{\partial}{\partial r}r\frac{\partial (q_r/r)}{\partial r} + \frac{1}{r^2}\frac{\partial^2 q_r}{\partial \theta^2} - \frac{q_r}{r^2} - \frac{2}{r^2}\frac{\partial q_\theta}{\partial \theta}\right) \tag{3}$$

$$\frac{\partial q_\theta}{\partial t} + \frac{\partial q_\theta q_z}{\partial z} + \frac{\partial q_r (q_\theta/r)}{\partial r} + \frac{1}{r^2}\frac{\partial q_\theta q_\theta}{\partial \theta} + \frac{q_\theta q_r}{r^2} = -\frac{\partial p}{\partial \theta} + \frac{1}{Re_p}\left(\frac{\partial^2 q_\theta}{\partial z^2} + \frac{\partial}{\partial r}r\frac{\partial (q_\theta/r)}{\partial r} + \frac{1}{r^2}\frac{\partial^2 q_\theta}{\partial \theta^2} - \frac{q_\theta}{r^2} + \frac{2}{r^2}\frac{\partial q_r}{\partial \theta}\right) \tag{4}$$

where, z, r, θ are respectively streamwise, wall-normal and azimuthal coordinates, and $q_z = u_z$, $q_r = ru_r$, $q_\theta = ru_\theta$, are three fluxes introduced to circumvent the singularity on the axis of the pipe (Orlandi, 2001). The equations are non-dimensionalised using the pipe radius R, and, the centreline streamwise velocity of the laminar Poiseuille flow at the initial flow condition, U_{p0}, and hence, $Re_p = RU_{p0}/\nu$. The spatial derivatives are discretized using a second-order central finite difference method. An explicit low-storage, third-order Runge–Kutta scheme is used for the temporal discretization of the nonlinear terms and a second order implicit Crank–Nicholson scheme is used for other terms. These are combined with the fractional-step method to enforce the continuity constraint (Kim and Moin, 1985). In this method, each time-advancement consists of three steps and the discretized equations are firstly solved for an intermediate non-solenoidal velocity field without a full consideration of the continuity constraint in each step. The Poisson equation is then solved for a virtual pressure field which is subsequently used to project the velocity field onto a solenoidal velocity field. Periodic boundary conditions are applied in the axial and azimuthal directions, and a non-slip boundary condition is imposed at the wall. The message passing interface (MPI) is used to parallelize the code. More detailed descriptions can be found in Seddighi (2011).

The pipe length has typically been chosen to be 10R in DNS of stationary (steady) flow simulations. According to Chin's (2011), however, this length is marginal for some statistics, such as *r.m.s.* of turbulent velocity and two-point correlation. Chin suggested a pipe length of $8\pi R$ to be used in order to ensure all statistics to be free from the effects of streamwise periodic boundary conditions. However, this length is overly strict. Wu and Moin (2008) used $15R$ as the pipe length in their simulations based on the findings that large scale motions (LSMs) range between $8R$ and $16R$. In the present study, the length of pipe is chosen to be $18R$ (corresponding to a viscous length of 3200 and 7800 for the initial and final flows, respectively). At this length, the statistical values converge for steady flows at both low ($Re_\tau = 180$) and high ($Re_\tau = 437$) Reynolds numbers, where $Re_\tau = Ru_\tau/\nu$, and u_τ is the friction velocity. In addition, the two point correlation of the streamwise velocity during the transient stages (shown in Fig. 6) reduces to zero within half of the streamwise domain, confirming the adequacy of the domain size in the flow direction.

The mesh employed here is $800 \times 160 \times 480$ ($z \times r \times \theta$). The mesh resolution at the initial Reynolds number ($Re_0 = 2650$, where $Re_0 = RU_{b0}/\nu$ and U_b is the bulk velocity; the subscript 0 refers to the initial flow and the subscript 1 refers to the final flow) is $\Delta z^+ = 4.5$, $\Delta r_{min}{}^+ = 0.09$, $\Delta r_{max}{}^+ = 2.4$, and $\Delta(r\theta)_{max}{}^+ = 2.4$. At the final Reynolds numbers ($Re_1 = 7362$), it is $\Delta z^+ = 9.8$, $\Delta r_{min}{}^+ = 0.22$, $\Delta r_{max}{}^+ = 6.0$, and $\Delta(r\theta)_{max}{}^+ = 5.6$. These are similar to the resolution used in HS2013. To validate the DNS code, steady simulation results at $Re_{\tau 0} = 180$ and $Re_{\tau 1} = 437$ are compared with the benchmark data of DNS (Fukagata and Kasagi, 2002) at $Re_\tau = 180$ and the experiment (Durst et al., 1995) at $Re_\tau = 410$ (Fig. 1). Our results show a good agreement with the benchmark data.

The rapid acceleration of the flow is implemented as follows: The initial and final flow Reynolds numbers are chosen at 2650 ($Re_{\tau 0} = 180$) and 7362 ($Re_{\tau 1} = 437$), respectively, which are close to the corresponding channel flow Reynolds numbers, 2825 ($Re_{\tau 0} = 178$) and 7404 ($Re_{\tau 1} = 418$) to facilitate a direct comparison. The subscripts 0 and 1 stand for initial flow and final flow, respectively. DNS of a flow at the initial Reynolds number is carried until the flow has reached fully developed statistically. Then, the flow is accelerated rapidly with

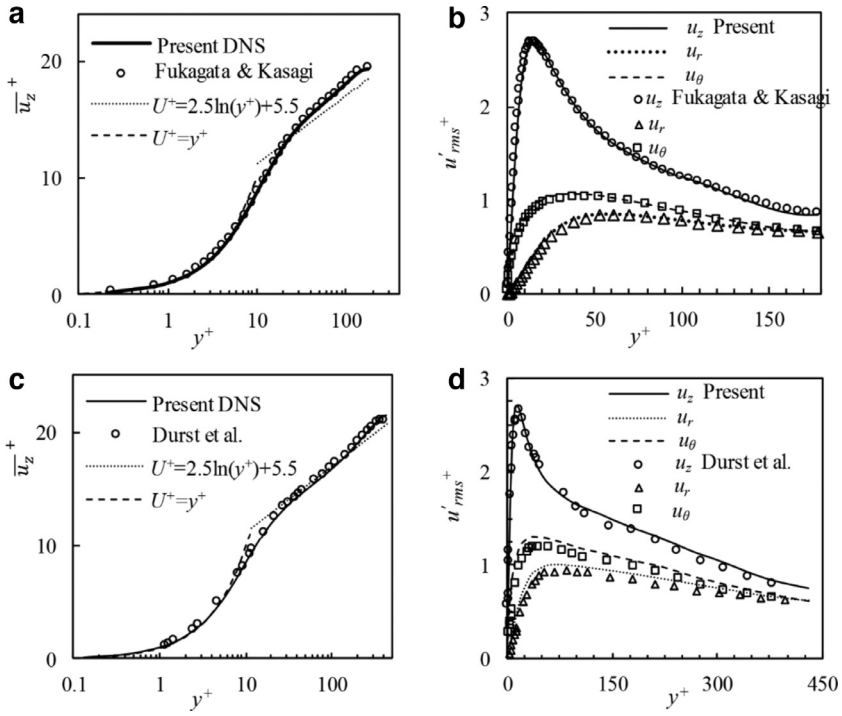

Fig. 1. Validation of the code for (a), (b) $Re_\tau = 180$ (c), (d) $Re_\tau = 437$.

a linear increase in its mass flow rate. The acceleration period is very short ($\Delta t^* = 0.22$, where $t^* = t\ U_{b1}/R$ and U_{b1} is the bulk velocity of the final flow). This can be compared with the Kolmogorov and the integral time scales of final flow which are about $t^* = 0.1$ and 0.9, respectively, and the period during which the flow is transient which is $t^* = 42$, as will be shown later. Consequently the flow can be seen as undergoing a step change. The simulation continues until the flow has become fully developed again ($t^* = 97$). The calculation of ensemble-averaged statistical quantities follows the method used in HS2013, through averaging in the two periodic directions and eight flow realizations. The initial flow for each simulation is selected from an instant of the steady state flow simulation at Re_0 and there is an interval of at least $\Delta t^* = 70$ between any two flow fields used, ensuring that the flow fields used in the ensemble averaging are independent of each other. The simulation results are re-scaled using the final flow bulk velocity (U_{b1}) or initial shear velocity ($u_{\tau 0}$) as will be indicated when they are presented. The purpose is to facilitate the discussion of the results and comparison with the data from HS2013.

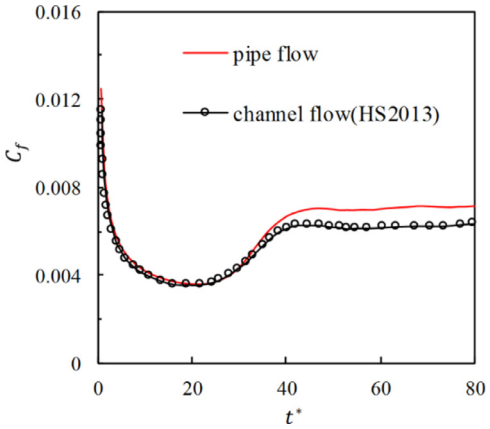

Fig. 2. Development of friction coefficient.

3. Results and discussion

3.1. Three stages of the transient pipe flow

As mentioned in Section 1, the transient process of a channel flow responding to a rapid flow acceleration can be described as a laminar–turbulent transition, comprising three distinct stages namely, pre-transition, transition, and fully turbulent stages. The three-stage process is reflected in the development of the friction coefficient, C_f ($C_f = \tau_w/0.5\rho U_0{}^2$) which also reflects the development of wall shear stress. Fig. 2 shows the development of C_f of the present pipe flow together with that of a channel flow for comparison. Prior to the commencement of the acceleration, the friction coefficient is equal to the value ($C_{f0} = 0.00928$) corresponding to the initial steady-state flow at $Re_0 = 2650$.

Immediately after the commencement of the acceleration, it increases rapidly to a much higher value, reaching a maximum at ($t^* = 0.22$ when the acceleration is terminated. The value then reduces gradually, reaching a minimum value at around $t^* = \sim 21$ or $t^{+0} = 92$ (the corresponding time for the channel flow is $t^* = 21$ or $t^{+0} = 90$). Subsequently, C_f recovers and approaches the steady flow value of the final flow around $t^* = 42$. Then, it only changes slightly until $t^* = \sim 50$, and remains constant afterwards. It is seen that the trend of the development of the friction factor is the same as that of the transient channel flow of HS2013. In fact, the friction factors of the two flows are practically the same before $t^* = 30$. In addition, the time for the transition onset is the same in the two flows. Similar to the channel flow, the response can be characterized into three stages; namely pre-transition ($t^* < 21$), transition ($t^* = 21$–42) and fully developed stage ($t^* > 42$).

The pre-transition is characterized by the formation of a thin boundary layer of a high strain rate on the wall, which then grows into the core of the flow with time. The existing turbulence serves as disturbances much like the FST in a boundary layer. The development of the boundary layer is shown in Fig. 3(a) and (b) in terms of momentum thickness Reynolds number and shape factor.

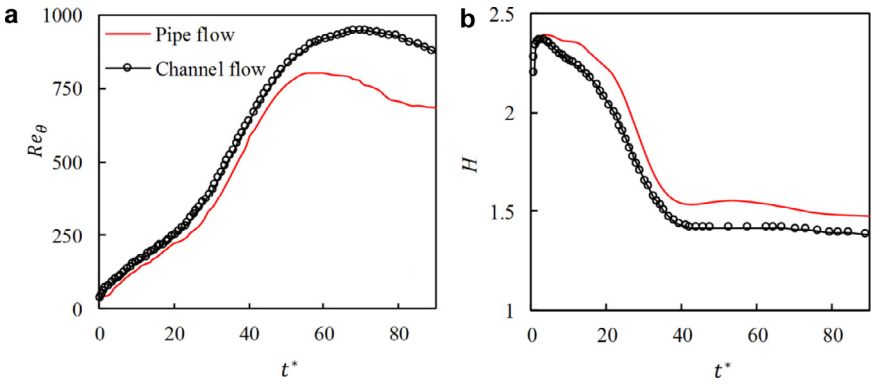

Fig. 3. Transient boundary layer behaviour of pipe flow and channel flow.

These are based on the perturbation velocity $\bar{u}^\wedge$ defined in a way similar to that used in HS2013, but it is modified for the cylindrical coordinate.

$$\bar{u}^\wedge(r,t^*) = \frac{\bar{u}(r,t^*) - \bar{u}(r,0)}{\overline{u_c}(t^*) - \overline{u_c}(0)} \tag{5}$$

$$R^2 - \left(R - \delta^*_{du}\right)^2 = \int_0^R (1 - \bar{u}^\wedge(r,t^*))2r\,dr \tag{6}$$

$$R^2 - \left(R - \theta_{du}\right)^2 = \int_0^R \bar{u}^\wedge(r,t^*)(1 - \bar{u}^\wedge(r,t^*))2r\,dr \tag{7}$$

$$Re_\theta = \frac{\theta_{du}\overline{u_c}(t^*)}{\nu} \tag{8}$$

$$H = \frac{\delta^*_{du}}{\theta_{du}} \tag{9}$$

where, $\bar{u}$ and $\overline{u_c}$ are ensemble-averaged local streamwise mean velocity and the centre velocity of the pipe flow, respectively.

Overall, the boundary layer in a pipe develops in a way similar to that of the channel flow. Re_θ grows almost linearly with time until $Re_\theta \approx 240$. Afterwards, the growth rate increases as a result of the onset of the transition. The value of Re_θ of the pipe flow is close to, but lower than that of the channel flow during the pre-transition and the transition periods, and diverges from it after the transition is completed ($t^* > 42$). That is, even though the values of Re_θ are significantly different in the two flows they are very close during the transition period. The shape factor of the pipe flow shows a similar developing pattern to that of the channel flow but with a higher value.

3.2. Instantaneous flow

Fig. 4 shows the contours of the streamwise fluctuating velocity u'_z at a r–θ plane ($z/R = 5.0$) and a z–θ plane ($y^{+0} = 5.4$, where y^{+0} is the radial distance from the wall normalized with $\nu/u_{\tau 0}$) at several instants following the rapid increase of flow rate. The first frame ($t^* = 0$) corresponds to the steady flow field just before the start of the transient flow. It is seen from the z–θ plane that the values of u'_z are relatively low and the colour is light. Some weak and short patches of high-speed (dark color) and low-speed (brighter color) patterns are present in the initial flow field. The r–θ plane shows that these streaks appear alternately in the azimuthal direction and the low speed streaks penetrate deeper into the core region of the pipe (Klebanoff et al., 1962). During $t^* = 0$–21, elongated streaks of positive and negative u_z' are formed and intensified. The r–θ plane plots on the left show that the low- and high-speed streaks are confined to the region very close to the wall. Later, some highly fluctuating velocities are seen to form, which appear as isolated turbulent patches (or, spots, see panel at t^*= 28). The spots spread into the flow and merge with each other until about $t^* = 42$, when the turbulence occupy the z–θ near plane.

To further illustrate the flow structures, Fig. 5 shows the iso-surface plots of u'_z/U_{b1} and λ_2 at $t^* = 0$, 14, 21, and 42. Only the bottom half of the pipe is displayed. λ_2 is the second eigenvalue of the symmetric tensor $\boldsymbol{S}^2 + \Omega^2$ where $\boldsymbol{S}$ and Ω are the symmetric and antisymmetric parts of the velocity gradient tensor ∇u. This value is introduced by Jeong and Hussain (1995) to identify vortex cores, and has been used frequently in studies of transition and turbulence. At $t^* = 0$, there are few short low- and high-speed streaks. At a later pre-transition stage ($t^* = 14$), elongated streaks appear alternately, which start to break up at $t^* = 21$ at some isolated places in the pipe. Packets of hairpin-like structures (identified by the iso-surface of the negative λ_2) are observed mostly surrounding the low-speed streaks. There are very few of such structures in the early pre-transition stage, and the size of such packet is small; but at $t^* = 21$, large spots of the turbulence start to occur, which signify the onset of transition. At the end of the transition ($t^* = 42$), fine vortical structures are full of the flow. The development of the streaky and vortical structures during the transient flow exhibits a great resemblance to that of the channel flow of HS2013.

The streamwise and spanwise correlation coefficients of the streamwise velocity, R_{11}, contain quantitative information of the streaky structures. Fig. 6(a) and (b) shows the profiles of R_{11} at several instants. It is seen that the magnitude of the negative value of the spanwise correlation increases slightly first and then remains largely unchanged during the early pre-transitional stage ($t^* = 4$–17). The minimum values of the pipe flow at onset of transition are -0.21, whereas those for channel and boundary layer flow are -0.3, and -0.35 respectively (HS2013). The distance at which the minimum R11 occurs decreases from the highest value ~0.3R (~$50\frac{\nu}{u_{\tau 0}}$) rapidly to a minimum ~0.23R (~$70\frac{\nu}{u_\tau}$, or ~$41\frac{\nu}{u_{\tau 0}}$) at pre-transition stage and it reduces to a value ~0.12R (~$50\frac{\nu}{u_\tau}$, or ~$122\frac{\nu}{u_{\tau 0}}$) at final steady stage. The averaged spanwise spacing of the streaks at the onset of transition is therefore approximately 0.46R (~$140\frac{\nu}{u_{\tau 0}}$), which is about twice the boundary thickness (based on $\bar{u}/\bar{u}_c$) and is different from the typical steady flow value of 0.6R (~$100\frac{\nu}{u_\tau}$). The growth of the streaks in streamwise can be observed from Fig. 6(b). The length of the streaks grows from ~3.5R (or ~$630\frac{\nu}{u_{\tau 0}}$) to ~4.5R (or ~$1350\frac{\nu}{u_\tau}$) at $t^* = 21$, showing the elongation of the streaks during the pre-transition period. It reduces to ~2.4R (or ~$1000\frac{\nu}{u_\tau}$) at the final stage ($t^* = 97$), commensurate with the characteristics of a steady turbulent flow at a higher Reynolds number.

3.3. Flow statistics

3.3.1. Mean velocity

Fig. 7 shows the profiles of the ensemble-averaged mean velocity profiles normalized by $u_\tau(t)$ at several instants. Also shown in the plot are the corresponding values of the channel flow. During the

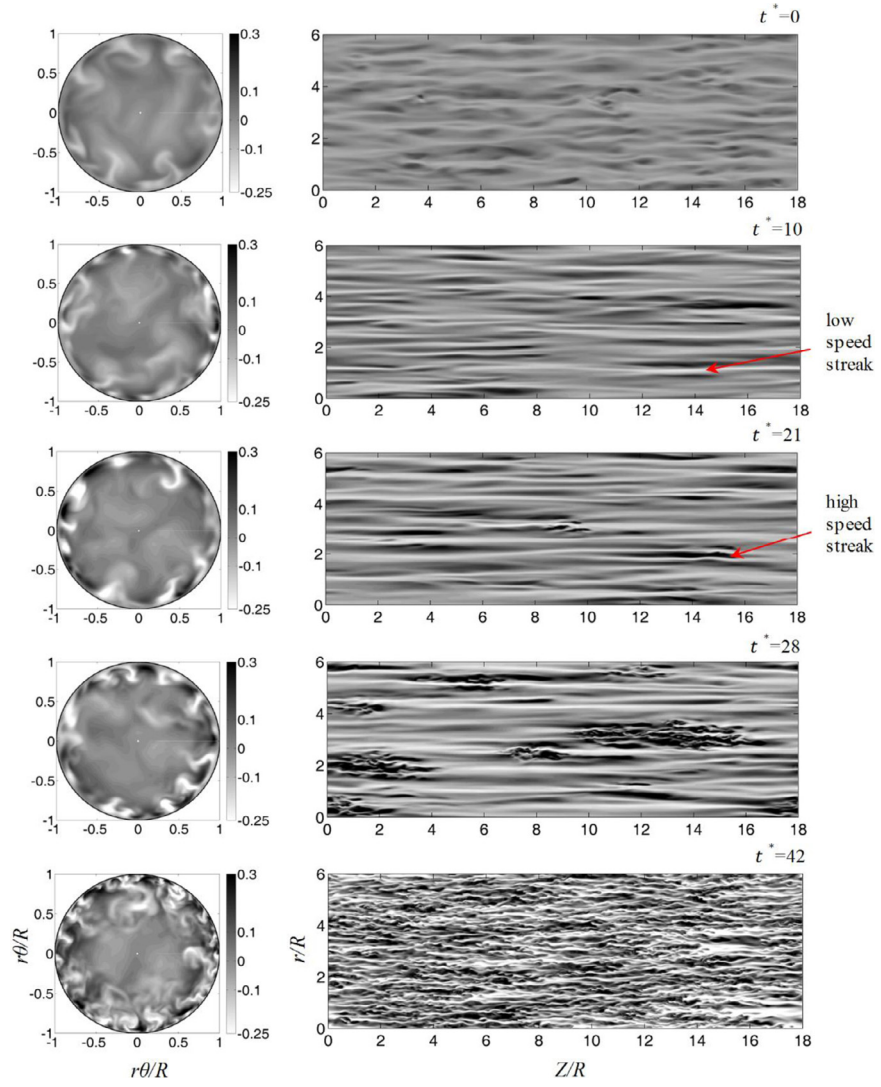

Fig. 4. Development of flow structure (2-D). Left: Contour plots of (u'_z/U_{b1}) in a r–θ plane ($z/R = 5.0$); right: contour plots of (u'_z/U_{b1}) in a z–θ plane ($y^{+0} = 5.4$). bright: low speed streaks; dark: high speed streaks.

pre-transitional period, after a rapid reduction at the very beginning, the velocity gradually increases with time reaching a maximum around the onset of the transition. During this period, the thickness of the sub-layer increases due to the growth of the boundary layer. During the transition period, the velocity in the core progressively reduces and the profile gradually approaches the typical distribution of a steady flow again. It can be seen that the behaviour of the velocity profiles in the pre-transition stage (Fig. 7(a)) is very similar to that in the channel flow. There are however some quantitative differences between two flows. At the initial steady flow, the velocity profiles in the pipe and channel flows overlap each other in $y^+ \leq 20$, but differ beyond this region.

During the pre-transition period, the profiles in the two flows are very similar. In a steady pipe flow, the velocity in the centre region is higher than that in the channel flow. The quantitative differences in the centre region still remain during the pre-transition period. This is due to the fact that both flows respond to the increase of the flow rate as a "plug" flow due to the 'inertia effect', namely, the velocity of the fluid is uniform across any cross-section of the pipe perpendicular to the axis of the pipe, and reduces rapidly to zero in the vicinity of the wall due to no-slip boundary condition on the wall. The turbulence in centre region is frozen so that the mean velocity profile does not change. During the transition period, the profiles of both the pipe and the channel flows reduce significantly in the log law region during $t^* = 28.8$–34.8. The quantitative differences reduce towards the later stage of the transition and at the end, the main differences between the two profiles are in the wake region.

3.3.2. Development of Reynolds stresses

Fig. 8 shows the development of the ensemble-averaged *r.m.s.* value of the fluctuating velocities normalized by the final bulk velocity ($u'_{z,rms}/U_{b1}$, $u'_{r,rms}/U_{b1}$, $u'_{\theta,rms}/U_{b1}$), together with the normalized Reynolds stress ($\overline{u'_z u'_r}/{U_{b1}}^2$). The curves with makers are data of channel flow at corresponding positions. The responses in the wall region (y^{+0}<36) are shown in Fig. 8(a), (c) and (e) and those in the core region are shown in Fig. 8(b), (d) and (f). It is clear that the response of turbulence is different in the wall and in the core regions. In addition, the response of the streamwise turbulence $u'_{z,rms}$ is characteristically different from those of the other two components. Focusing on the streamwise turbulence first, the values of $u'_{z,\,rms}$ in the wall region ($y^{+0} = 8.6$, 19.5) increase rapidly with small or no delays until $t^* < 34$, after which they reduce and eventually approach the steady state values. The response of $u'_{z,\,rms}$ at other locations all have some delays before increasing, the length of which increases with the distance from the wall. In the wall and buffer regions, $u'_{z,\,rms}$ over-shoots its final steady values at $t^* = \sim 30$. The responses of $u'_{r,rms}$ and u'_θ are similar to each other, but are distinctively different from that of the $u'_{z,\,rms}$ in the wall and buffer layers ($y^{+0} < 36$). They either

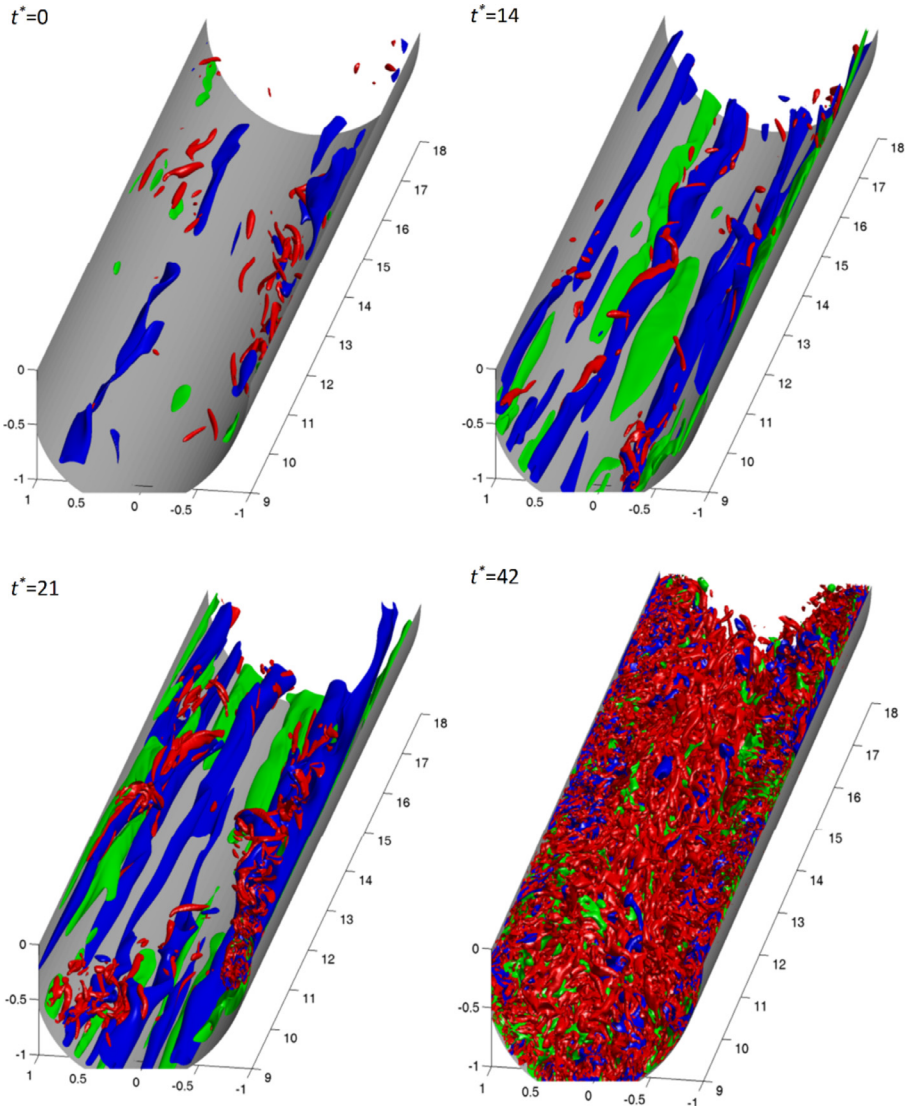

Fig. 5. Development of the streaks and vortex structures at several instants: 3-D iso-surfaces plots of low- and high-speed streaks (blue for $u_z'/U_{b1} = -0.13$ and green for $u_z'/U_{b1} = 0.13$); λ_2 (red for $\lambda_2 = -2$, normalized by $(u_{p0}/R)^2$). (For interpretation of the references to colour in this figure legend, the reader is referred to the web version of this article.)

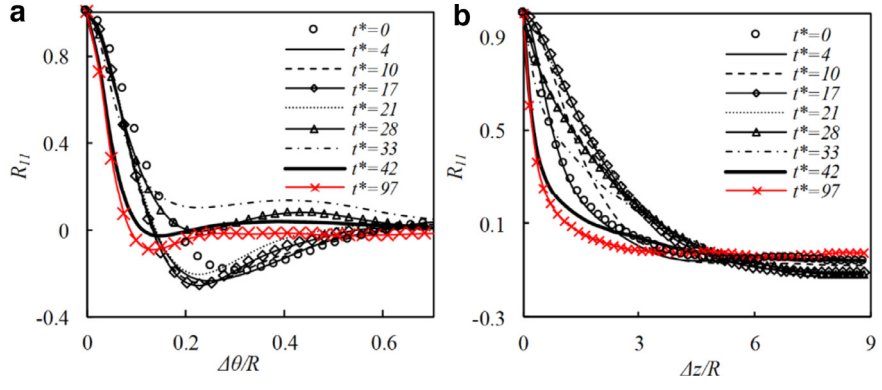

Fig. 6. Profiles of spanwise (a) and streamwise (b) correlations of the streamwise velocity at $y^{+0} = 5.4$.

reduce then increase slightly or remain more or less unchanged until $t^* = \sim 21$.

They then respond rapidly and reach to their corresponding final steady values (or slightly over-shooting them) just after $t^* = \sim 35$. In the core region, the response of $u'_{r,rms}$ and $u'_{\theta,rms}$ are similar to that of $u'_{z,rms}$, which show a delay followed by a period of response and the period of the delay is longer as the distance to wall increases. The Reynolds stress in Fig. 8(g) and (h) exhibits similar features described for the normal stresses.

The general behaviour of the responses of the various turbulence components is very similar to that observed by He and Jackson (2000) who studied much slower accelerated flows in a pipe experiment, but

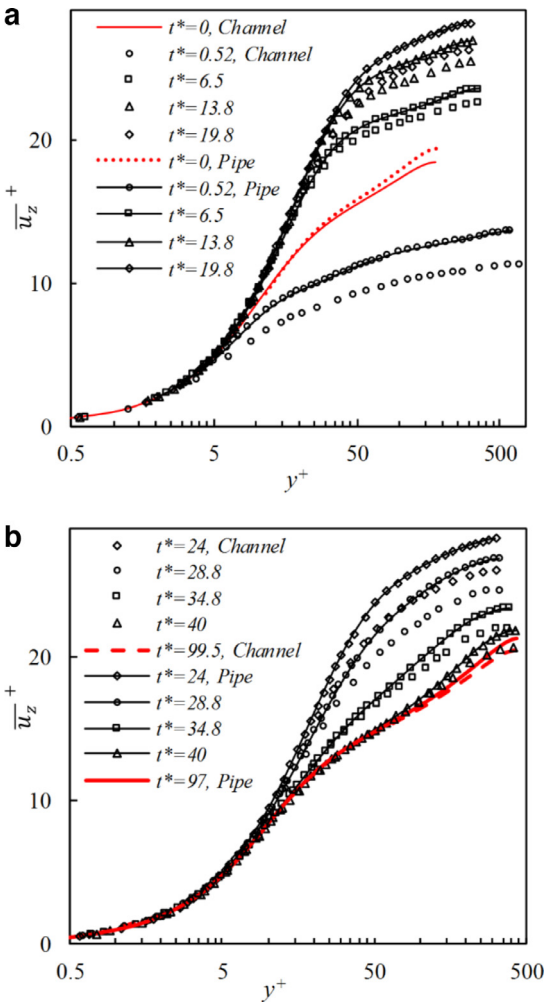

Fig. 7. Development of ensemble-averaged streamwise mean velocity: (a) pre-transition stage (b) transitional and fully developed stage.

their measurements were largely limited to the core and the buffer region (up to $y^{+0} \sim 17$). The turbulence behaviour was explained by relating them to turbulence production, energy redistribution between its components and the radial diffusion. The results in Fig. 8 provide detailed information in the wall region ($y^{+0} < 36$). More importantly, the present results show that the initial response in $u'_{z,rms}$ is due to the formation of elongated streaks which are not conventional turbulence. The rapid increase of $u'_{r,rms}$ and $u'_{\theta,rms}$ at around $t^* = \sim 21$ is linked to the transition of the flow, from an agitated laminar flow to a turbulent flow. This is to some extend related to the energy redistribution identified by He and Jackson (2000).

Comparing the pipe flow with the channel flow, the overall behaviour identified here is very similar. Especially, in the near wall region, the transient behaviour of $u'_{z,rms}$ is quantitatively similar before $t^* < 25$. However, some notable differences are observed in the centre region. Firstly, $u'_{z,rms}$, $u'_{r,rms}$, $u'_{\theta,rms}$ at $y^{+0} = 148$ increase earlier in pipe flow than in the channel flow. Secondly, the growth rates of $u'_{r,rms}$ and $u'_{\theta,rms}$ are similar before the onset of transition, however they become larger after the onset of transition in the pipe flow. One possible reason for these differences is that the structures are free to grow in spanwise in the channel flow, whereas in the pipe flow, the structures near the core region are constrained in the azimuthal direction. Stronger structure interactions in the pipe core region hence intensify the mixing of the flow, introducing an earlier growth of fluctuation velocities and a higher growth rate.

The growth rate of the peak *r.m.s.* of the fluctuating velocity represents the energy growth in the pre-transition stage. Fig. 9 shows the development of the streamwise fluctuating velocity normalised by its corresponding peak value in pipe flow, against $y/\delta_u{}^*$, where $\delta_u{}^*$ is defined as follows:

$$\bar{u}(r,t^*) = \frac{\overline{u}(r,t^*)}{\overline{u_c}(t^*)} \tag{10}$$

$$R^2 - (R-\delta_u^*)^2 = \int_0^R (1-\bar{u}(r,t^*))2rdr \tag{11}$$

The position of the peak value moves rapidly outwards at the beginning, then remains almost unchanged at 0.75 $\delta_u{}^*$ during t^*=5–21. It is of interest noting that the location of the peak value of the transient pipe flow is similar to that found for the channel flow, which remains unchanged during $t^* = 5$–21 at $0.75\delta_u{}^*$. As indicated by HS2013, this behaviour suggests that $u'_{z,rms}$ value varies with the growth of the boundary layer and can be scaled with boundary thickness instead of the inner scaling. This is in fact an important feature of the boundary bypass transition reported (e.g. Cossu et al., 2009).

Fig. 10(a) and (b) shows the growth of square of the peak *r.m.s.* of fluctuating velocities together with the turbulent kinetic energy for both the pipe and channel flows. It is clear that following a short delay, the peak value grows linearly during pre-transition. It is estimated that at the onset of transition, the streak amplitude ($u'_{z,rms}$) grows to ~14% of mean flow, which is the same as that of the channel flow (HS2013). The growth rates of the pipe and channel flows are the same before $t^* < 21$. However, after that, and the growth rates of all components are different in the two flows.

3.3.3. Turbulent viscosity

Fig. 11 shows the development of turbulent viscosity (μ_t) calculated from

$$\mu_t = \frac{\rho\overline{u'_z u'_r}}{d\overline{u_z}/dy} \tag{12}$$

The turbulent viscosity reflects turbulent activities and mixing, and useful parameter in RANS modelling. It can be seen from Fig. 11(a) that during $t^* = 0$–19.5, the value of μ_t/μ in the core region ($y^{+0} > 60$) remains more or less unchanged (except for some fluctuations) but it decreases in the wall region ($y^{+0} < 60$). During the transition period ($21 < t^* < 42$), μ_t/μ increases rapidly near the wall ($y^{+0} < 60$), reaching its final steady values towards the end of this period (see Fig. 11(b)). The increase of μ_t/μ in the core region is much slower, which continues after the completion of transition ($t^* = 43$). The behaviour of μ_t/μ in the channel is generally the same with that of the pipe flow. The steady state value is slightly lower in the pipe flow than in the channel flow, especially in the centre region ($y^{+0} > 50$). It is interesting to see that this difference in the centre region ($y^{+0} > 50$) is reduced during the transition stage ($21 < t^* < 43$), but it is regained when the flow is fully developed again. As indicated in Section 3.3.2, the growth of turbulent shear stress ($\overline{u'_z u'_r}$) in the centre region is different for the two types of flows during the transition stage. The value of $\overline{u'_z u'_r}$ grows faster in the pipe flow at this stage. However, this is not reflected in the turbulence viscosity response, which implies different growth behaviours of velocity gradient in the two flows. This is discussed in the next section.

3.3.4. Vorticity Reynolds number

Gorji et al. (2014) showed that the $\gamma - Re_\theta$ transitional model can predict the basic features of a ramp-up flow rather well. However, the predicted onset of the transition in three ramp-up flow cases by this model is noticeably delayed. A key feature of this turbulence model is to make use of the correlation between Re_θ and $Re_{v.max}$, replacing the former by the latter to trigger the transition. The correlation will

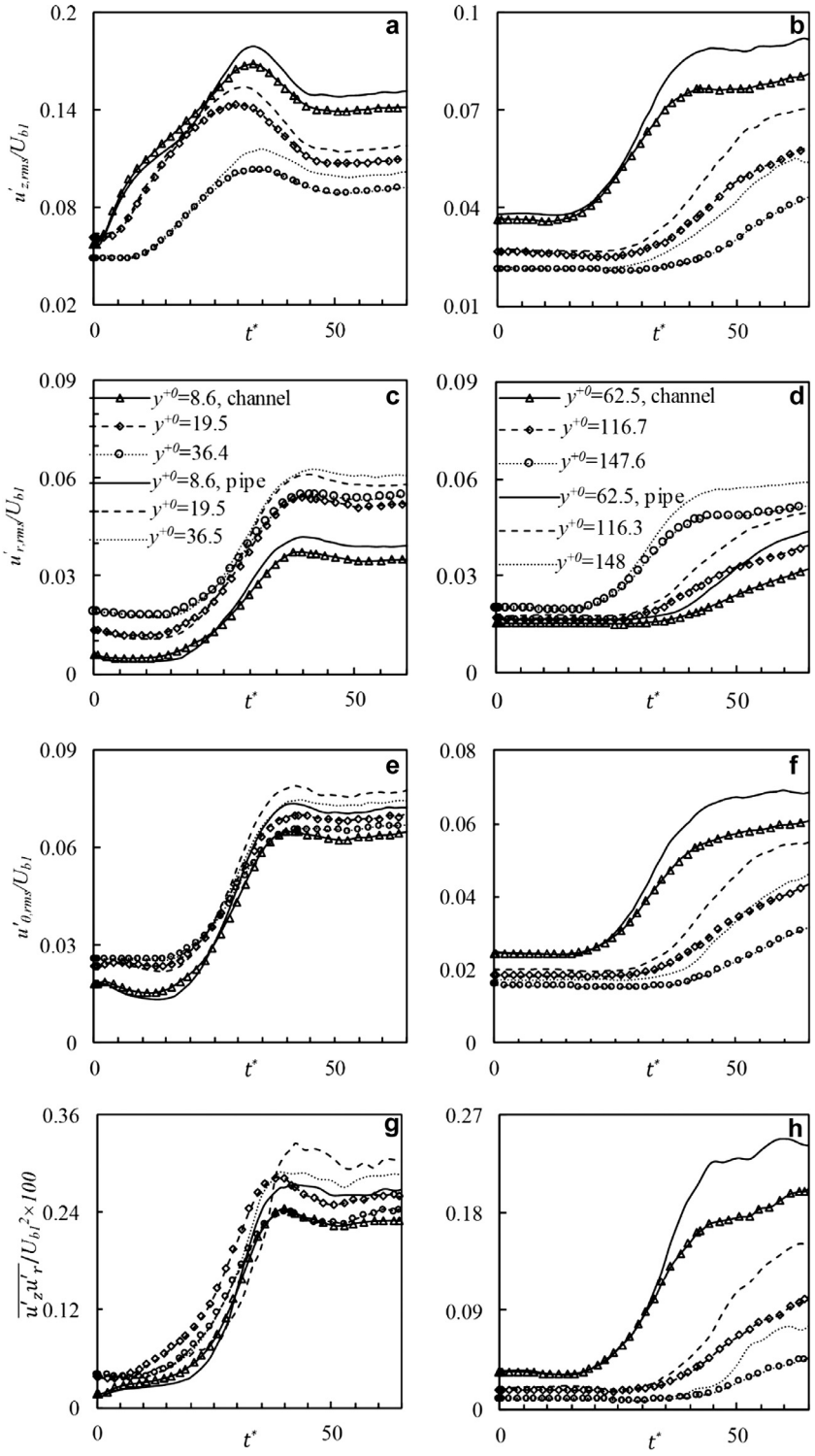

Fig. 8. Development of the normalized *Reynolds stresses*. (a, c, e, g) near-wall region; (b, d, f, h) core region. Lines: pipe flow, lines with makers: channel flow.

be evaluated in this section. The vorticity Reynolds number Re_v was originally defined by van Driest and Blumer (1963). It reads

$$Re_v = \frac{\rho y^2}{\mu}\frac{d\overline{u_z}}{dy} \tag{13}$$

where $\overline{u_z}$ is the local mean velocity. It is known that (Driest and Blumer, 1963; Langtry, 2006) the maximum value of this local parameter ($Re_{v.max}$) can be directly linked to the momentum thickness Reynolds number Re_θ through an empirical correlation. Hence $Re_{v.max}$ is used in favour of Re_θ to avoid the integration of the boundary layer velocity profile in order to determine the onset of transition in the RANS approaches. In the Blasius boundary layer, the maximum Re_v in the wall-normal direction is proportional to the momentum thickness Reynolds number as $Re_{v.max} = 2.193Re_\theta$. For a flat plate boundary layer flow, it is shown that the constant in the correlation is affected by pressure gradient. The error is less than 10% when the flow is subjected to a pressure gradient which varies the shape factor between 2.3 and 2.9 (Langtry, 2006).

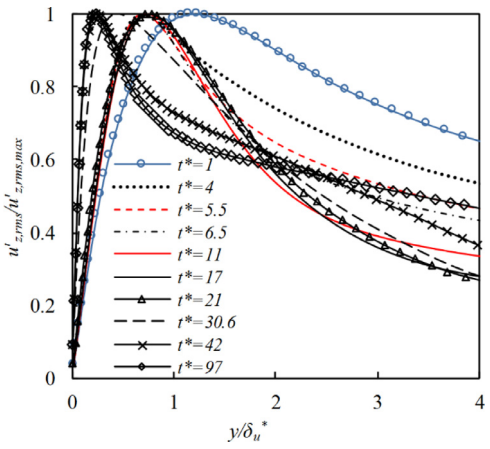

Fig. 9. Development of u_{rms} normalized by the peak value.

Fig. 12(a) and (b) shows the developments of the vorticity Reynolds number (Re_v) in the channel and pipe flows. The calculation of Re_v is based on local mean velocity. It is shown in Fig. 12(a) that this local parameter increases quickly near the wall ($y/R < 0.4$), forming a local peak. Another peak is observed at the centre, however, it does not respond to the flow rate change. This is consistent with earlier observations that there are no structural changes in centre region. Fig. 12(b) shows that Re_v in the centre ($y/R > 0.4$) increases quickly during the transition stage, whereas Re_v near the wall starts to decrease. In Fig. 12(c), the development of peak Re_v against the Re_θ in pipe flow is shown, where Re_θ is calculated from the local mean velocity. It is found that the relationship between $Re_{v.max}$ and Re_θ is not linear. The values of Re_θ and $Re_{v.max}$ at the onset of transition are 395 and 281, respectively.

Let us now consider the differential velocity ($\tilde{u}\hat{}$ defined in Section 3.1). The correlations between $Re_{v.max}(\tilde{u}\hat{})$ and $Re_\theta(\tilde{u}\hat{})$, which are calculated from the differential velocity are calculated for both the pipe and channel flows. Fig. 12(d) shows that the near wall peaks, $Re_{v.max}$ of the pipe and channel flows both increase linearly with the Re_θ for $t^* < 14$. After that, $Re_{v.max}$ in the pipe flow increases slightly slower than Re_θ until $t^* = 19.8$. In the transitional stage, $Re_{v.max}$ increases significantly slower than Re_θ. It shows that there is a linear relationship between Re_θ and $Re_{v.max}$ at the pre-transition stage if these parameters are calculated from the differential mean velocity. The linear correlation between the $Re_{v.max}$ and Re_θ in the transient pipe and channel flows are respectively as:

$$Re_{v,max} = 0.99Re_\theta \tag{14}$$

$$Re_{v,max} = 0.62Re_\theta \tag{15}$$

The differences between the actual momentum thickness Reynolds number and the prediction of equations are less than 22%

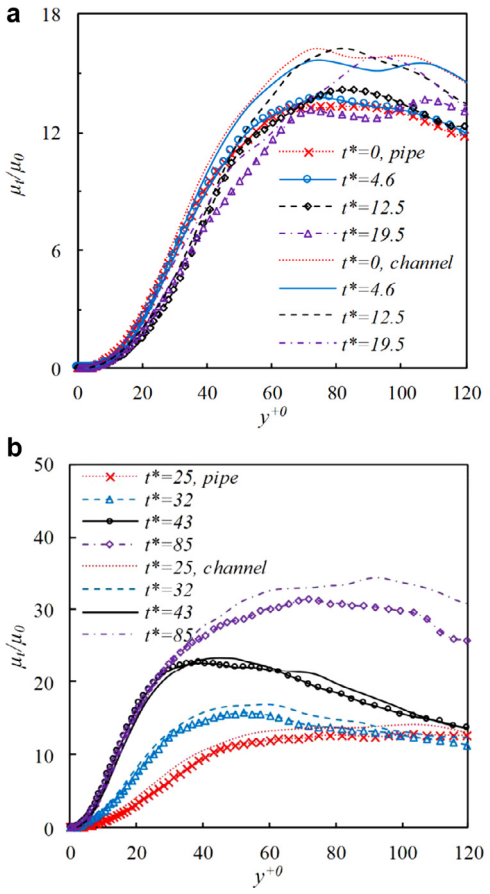

Fig. 11. Development of turbulent viscosity: (a) pre-transition stage (b) transition and fully turbulent stages.

and 14% respectively for the two equations during the pre-transition region ($t^* = 0$–19.8). As shown in Section 3.1, the growth of Re_θ is the same in the channel and pipe flows during pre-transition. The difference between the $Re_{v.max}$– Re_θ correlation in the two flows is therefore attributed to the different growth rates of the vorticity Reynolds number, which are in turn due to the different growths of the velocity gradient in these flows. Initially ($t^* = 0$–14), the growth of the velocity gradient of the pipe flow is faster than that of channel flow, but later ($t^* = 14$–19.8), the growth of velocity gradient of pipe flow slows down dramatically, contrasting to the steady growth of the velocity gradient in channel flow.

Consequently, the $Re_{v.max}$–Re_θ correlation is geometry dependent. This may have some implications when the models developed based on the boundary layer correlation are directly used for a

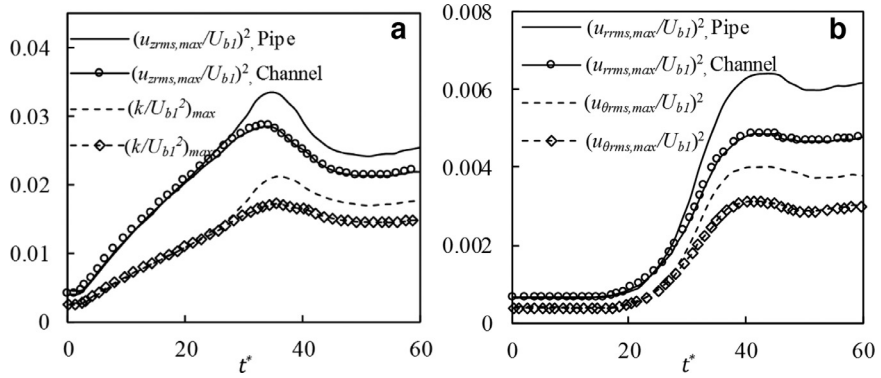

Fig. 10. History of squared of the peak *r.m.s. fluctuating* velocities. (a) u'_z and k (b) u'_r and u'_θ.

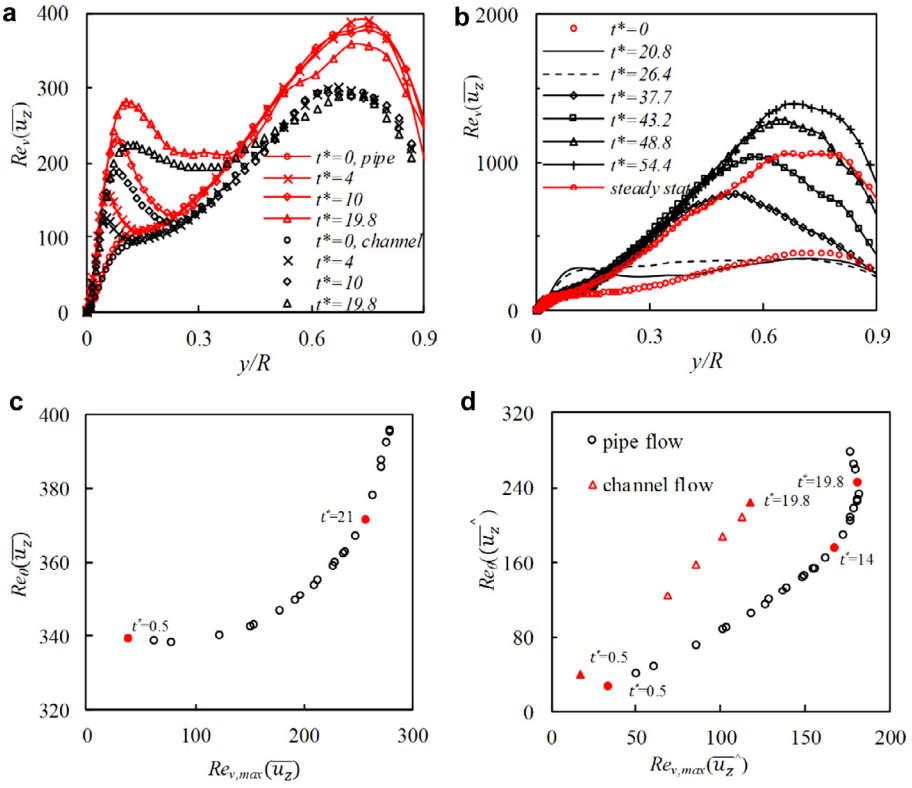

Fig. 12. Development of vorticity Reynolds number (Re_v). (a) Pre-transition; (b) transition and fully turbulent stages; (c) relationship between $Re_{v,max}$ and Re_θ at pre-transition stage (based on local mean velocity); (d) relationship between $Re_{v,max}$ and Re_θ at pre-transition stage (based on differential mean velocity). Lines with makers: pipe flow; makers: channel flow.

channel, pipe or other internal flows. Further studies are required to develop a better understanding.

3.3.5. Budget terms

In this section, we present the variations of the budget terms of $\overline{u'_z u'_z}$ during the transition period. The transport equation of $\overline{u'_z u'_z}$ in a cylindrical coordinate system is as follows:

$$\frac{\partial \overline{u'_z}^2}{\partial t} = -2\overline{u'_r u'_z}\frac{\partial \overline{u_z}}{\partial r} + 2\overline{p'\frac{\partial u'_z}{\partial z}} - 2\overline{\frac{\partial p' u'_z}{\partial z}} - \frac{2}{Re}\left[\overline{\left(\frac{\partial u'_z}{\partial z}\right)^2} + \overline{\left(\frac{\partial u'_z}{\partial r}\right)^2} + \frac{1}{r^2}\overline{\left(\frac{\partial u'_z}{\partial \theta}\right)^2}\right] - \frac{1}{r}\frac{\partial r\overline{u'_r {u'_z}^2}}{\partial r} + \frac{1}{Re}\left[\frac{1}{r}\frac{\partial}{\partial r}\left(r\frac{\overline{u'_z}^2}{\partial r}\right)\right] \quad (16)$$

On the right hand side of the equation, the terms from left to right are production, pressure strain, pressure diffusion, dissipation rate, turbulent transport and viscous diffusion, respectively. The pressure diffusion term is 0, which is not studied in the following section.

Fig. 13 shows the budget terms of $\overline{u'_z u'_z}$ normalized with ${u_\tau}^4 R/\nu$ at $t^* = 5.6, 11, 20, 25, 33, 42$. The budget terms of the final steady flow ($t^* = 97$) are shown for comparison. Since the data is normalized using the ensemble-averaged friction velocity (u_τ) at the corresponding t^*, the absolute variations during the transitional period cannot be shown. Instead, they show how the distributions deviate from those of a fully developed flow. At the beginning of the transient ($t^* = 5.6$), the budget terms are very low compared to the final flow results. This is due to the rapid increase of the wall shear stress.

There are characteristic differences between the budget distributions in the transient flow and in a steady turbulent wall shear flow. Firstly, the location of the peak production moves from $y^+ = 10$ in steady flow to $y^+ = 20$. Secondly, the dissipation term remains rather uniform in the wall region (say, $y^+ < 20$), whereas a typical feature of the wall shear flow is that the dissipation increases as the wall is approached. Thirdly, as noted before, the pressure–strain term remains very low compared to the production term, which implies that little energy is supplied to $\overline{u'_r u'_r}$ and $\overline{u'_\theta u'_\theta}$. These features of the budget terms are related to the fact that the "turbulence" generated during the pre-transition stage is not conventional turbulence, but due to the elongated streaky structures ($t^* < 20$).

Fig. 13(f) shows the response of the production (P), pressure strain (Π) and dissipation (ε) terms integrated over $y^{+0} \approx 0$–50 and $y^{+0} \approx 50$–100 respectively. All three terms are normalized with ${Ru_{\tau 0}}^4/\nu$ to show the absolute value of the development of these terms in the two regions. During the pre-transition period ($t^* < 21$), the pressure strain term remains unchanged in both regions. The production and dissipation terms grow steadily in the near wall region, but no significant changes are observed in central region. The production term is mainly balanced by the dissipation term at pre-transition stage in the near wall region, whereas it is balanced by both the pressure strain term and dissipation term in the central region. The values of the three terms in centre region are multiplied by 7 for clearer display. Therefore, the production and dissipation terms in the near wall region are much larger than those in the centre region for the flow studied herein.

The growths of the budget terms in the near wall region during the early period ($t^* < 20$) are not associated with conventional turbulence, but a reflection of the streaks developed in the region of $y^{+0} \approx 0$–50. Later during the transition period ($t^* = 21$–40), the growth rates of the three terms increase significantly in the near wall region. In the centre region, the growths of these terms are delayed until $t^* = 30$ when the pressure strain term starts to increase

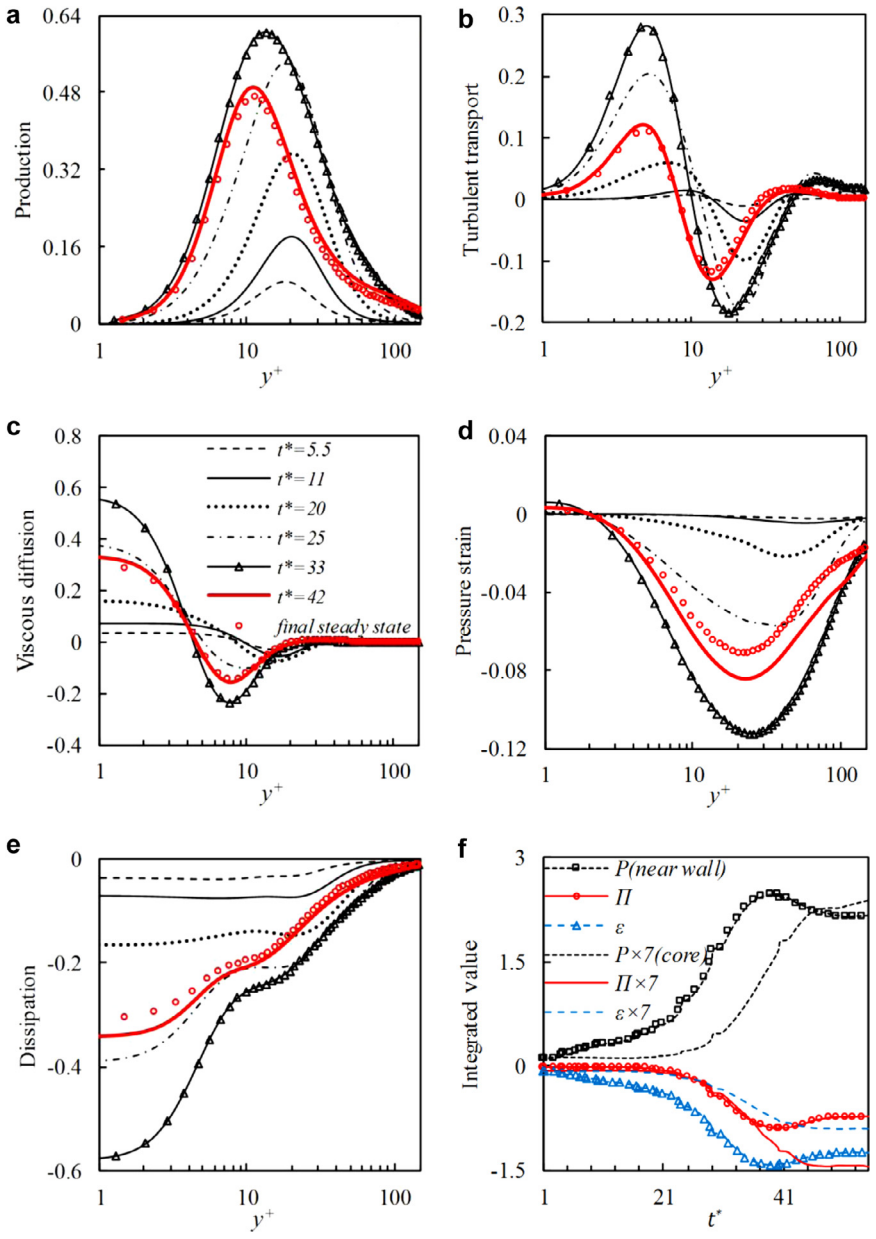

Fig. 13. Development of budget terms of $\overline{u_z'u_z'}$: (a) production; (b) turbulence transport; (c) visocus diffusion; (d) pressure strain; (e) disssipation; (f) Spatial integration of (a, d, e) in the wall and core regions.

significantly. The dominant terms are still production and dissipation in the region of $y^{+0} \sim 0$–50. However, the pressure strain term increases to a significant level in both the near wall and the central regions. It starts to overtake the dissipation for $t^* > 40$ in the region of $y^{+0} \sim 50$–100, where it redistributes a significant amount of energy from the streamwise component to the other two components. The budget terms reach a peak at $t^* \approx 40$, and then they drop to the steady state values at $t^* \approx 44$.

3.3.6. *Effect of starting and final Reynolds numbers*

The results discussed so far have been for a fixed starting and final Reynolds number. An interesting question to ask is that what will happen if the starting or the final Reynolds numbers are changed. Potentially, the transient process may be affected by a number of factors, including the initial turbulence characteristics (dependent on Re_0), the 'free stream' velocity (dependent on Re_1), the change rate of the mean velocity (dependent on $(U_{b1} - U_{b0})/\Delta t$), and the free stream turbulence level (dependent on Re_0 and Re_1). The rate of change of the mean velocity plays a weak role as long as the acceleration time is much less than the onset time of the transition (HS2013). It was shown that, in a channel flow, the critical Reynolds number $Re_{t,cr}$ $(= t_{cr}{}^* Re_1)$ is proportional to $Tu_0{}^{-1.71}$, where $t_{cr}{}^*$ is the time for the onset of transition, Tu_0 is defined as $(u'_{rms0,max})/U_{b1}$, $u'_{rms0,max}$ is the peak value of the *r.m.s.* of the streamwise fluctuating velocity of the initial flow. In Fig. 14, the results of three cases of pipe flows with the same initial Reynolds number ($Re_0 = 2650$) but different final Reynolds numbers ($Re_1 = 3000$, 5220, 7362) are plotted against the data obtained from channel flows (He and Seddighi, 2015). Those cases are simulated with the same mesh setup described in Section 2 for the case ($Re = 2650$–7362).

It can be seen from Fig. 14 that the critical Reynolds number for the pipe flow collapses extremely well with the correlation of the channel flow. The correlation developed for the channel transient flow, $Re_{t,cr} = 1340 Tu_0{}^{-1.71}$, can be also used for the pipe flow. For detailed discussion, the reader is referred to the study on transient channel flow (He and Seddighi, 2015).

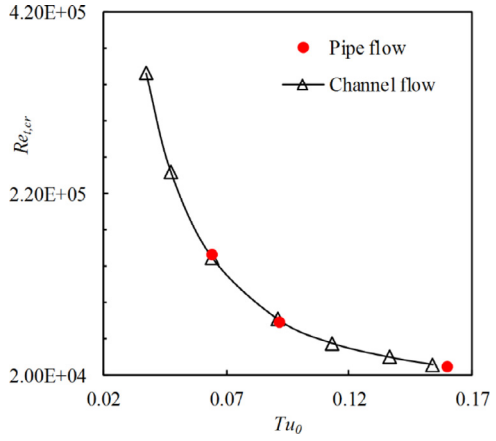

Fig. 14. Transition onset Reynolds number against Tu_0.

4. Conclusions

It has been shown that, similar to that in a channel, the transient flow in a pipe after a step increase in flow rate is effectively a laminar flow followed by a bypass transition. New turbulence generated through bypass transition mechanisms initially occupies the near wall region; it propagates into the centre region following the completion of the transition. The general trends of the transition in the pipe and channel flows are found to be the same in the near-wall region. The similarities among the two flows are not only in instantaneous flow structures, but also in the ensemble-averaged statistical values. However, there are detailed differences in the central region between the two flows during the transition stage. The growth of turbulence in the pipe at this stage is faster than that in the channel. This is attributed to the stronger mixing effect in the pipe, where the spanwise space becomes narrower as the flow goes closer to the centre. The developments of the mean velocity profiles, turbulent viscosity, vorticity Reynolds number and budget terms are analysed. It is found that the growths of the turbulent viscosity and the vorticity Reynolds number are quantitatively different in the two flows, which are attributed to the differences in the velocity gradient developments. These results may provide useful information for the development of turbulence models.

Acknowledgements

We gratefully acknowledge that the work reported herein is partially funded by UK Engineering and Physical Sciences Research Council (Grant No. EP/G068925/1). KH is jointly sponsored by Chinese Scholarship Council and The University of Sheffield.

References

Akhavan, R., Kamm, R.D., Shapiro, A.H., 1991. An investigation of transition to turbulence in bounded oscillatory Stokes flows. Part 1. Experiments. J. Fluid Mech. 225, 395–422.
Andersson, P., Berggren, M., Henningson, D.S., 1999. Optimal disturbances and bypass transition in boundary layers. Phys. Fluids 11, 134.
Brandt, L., Schlatter, P., Henningson, D.S., 2004. Transition in boundary layers subject to free-stream turbulence. J. Fluid Mech. 517, 167.
Colombo, A.F., Lee, P., Karney, B.W., 2009. A selective literature review of transient-based leak detection methods. J. Hydro-environment Res. 2, 212.
Choi, K.-S., Roach, P., DeBisschop, J.R., Clayton, B., 1997. Turbulent boundary-layer control by means of spanwise-wall oscillation. AIAA Paper 97-1795.
Chin, C., 2011. Numerical Study of Internal Wall-bounded Turbulent Flows. The University of Melbourne (Ph.D. thesis).
Cossu, C., Pujals, G., Depardon, S., 2009. Optimal transient growth and very large-scale structures in turbulent boundary layers. J. Fluid Mech. 619, 79.
Durst, F., Jovanovic, J., Sender, J., 1995. LDA measurements in the near-wall region of a turbulent pipe flow. J. Fluid Mech. 295, 305.
Driest, E.V., Blumer, C.E, 1963. Boundary layer transition: Free stream turbulence and pressure gradient effects. AIAA J. 1, 1303.
Fransson, J.H.M., Matsubara, M., Alfredsson, P.H., 2005. Transition induced by free-stream turbulence. J. Fluid Mech. 527, 1.
Fukagata, F., Kasagi, N., 2002. Highly energy-conservative finite difference method for the cylindrical coordinate system. J. Comput. Phys. 181, 478.
Ghidaoui, M.S., Zhao, M., McInnis, D.A., Axworthy, D.H., 2005. A review of water hammer theory and practice. Appl. Mech. Rev. 58, 49.
Greenblatt, D., MOSS, E.A., 2004. Rapid temporal acceleration of a turbulent pipe flow. J. Fluid Mech. 514, 65–75.
Gorji, S., Seddighi, M., Ariyaratne, C., Vardy, A.E., Donoghue, T.O., Pokrajac, D., He, S., 2014. A comparative study of turbulence models in a transient channel flow. Comput. Fluids 89, 111.
He, S., Jackson, J.D., 2000. A study of turbulence under conditions of transient flow in a pipe. J. Fluid Mech. 408, 1.
He, S., Jackson, J.D., 2009. An experimental study of pulsating turbulent flow in a pipe. Eur. J. Mech. B/Fluids 28, 309.
He, S., Ariyaratne, C., Vardy, A.E., 2008. A computational study of wall friction and turbulence dynamics in accelerating pipe flows. Comput. Fluids 37, 674.
He, S., Seddighi, M., 2013. Turbulence in transient channel flow. J. Fluid Mech. 715, 60.
He, S., Seddighi, M., 2015. Transition of transient channel flow after a change in Reynolds number. J. Fluid Mech. 764, 395.
Jacobs, R.G., Durbin, P.A., 2001. Simulations of bypass transition. J. Fluid Mech. 428, 185.
Jeong, J., Hussain, F., 1995. On the identification of a vortex. J. Fluid Mech. 285, 69.
Kataoka, K., Kawabata, T., Miki, K., 1975. The start-up response of pipe flow to a step change in flow rate. J. Chem. Eng. Japan 8, 266.
Kim, J., Moin, P., 1985. Application of a fractional-step method to incompressible Navier–Stokes equations. J. Comput. Phys. 59, 308.
Klebanoff, P.S., Tidstrom, K.D., Sargent, L.M., 1962. The three-dimensional nature of boundary-layer instability. J. Fluid Mech. 12, 1.
Langtry, R.B., 2006. Correlation-based Transition Modelling for Unstructured Parallelized Computational Fluid Dynamics Codes. University of Stuttgart (Ph.D. thesis).
Maurizio, Q., Stefano, S., 2000. Numerical simulation of turbulent flow in a pipe oscillating around its axis. J. Fluids Mech. 424, 217–241.
Maruyama, T., Kuribayashi, T., Mizushina, T., 1976. The structure of the turbulence in transient pipe flows. J. Chem. Eng. Japan 9 (6), 431–439.
Meseguer, A., Trefethen, L.N., 2003. Linearized pipe flow to Reynolds number 10^7. J. Comput. Phys. 186, 178.
Mizushina, T., Maruyama, T., Hirasawa, H., 1975. Structure of the turbulence in pulsating pipe flow. J. Chem. Eng. Japan. 8 (3), 210–216.
Mankbadi, R.R, Liu, J.T.C., 1992. Near-wall response in turbulent shear flows subjected to imposed unsteadiness. J. Fluid Mech. 238, 55–71.
Nagarajan, S., Lele, S.K., Ferziger, J.H., 2007. Leading edge effect in bypass transition flow. J. Fluid Mech. 572, 471.
Nagib, H.M., Chauhan, K.A., 2008. Variations of von Kármán coefficient in canonical flows. Phys. Fluids 20, 101518.
Ovchinnikov, V., Choudhari, M.M., Piomelli, U., 2008. Numerical simulations of boundary-layer bypass transition due to high-amplitude free-stream turbulence. J. Fluid Mech. 613, 135.
Orlandi, P., 2001. Fluid Flow Phenomena: A Numerical Toolkit, 2001. Kluwer.
Seddighi, M., He, S., Vardy, A.E., Orlandi, P., 2014. Direct numerical simulation of an accelerating channel flow. Flow Turbul. Combust. 92, 473.
Seddighi, M., He, S., Vardy, A.E., Orlandi, P., 2011. A comparative study of turbulence in ramp-up and ramp-down unsteady flows. Flow Turbul. Combust. 86, 439–454.
Seddighi, M., 2011. Study of Turbulence and Wall Shear Stress in Unsteady Flow over Smooth and Rough Wall Surfaces. University of Aberdeen (Ph.D. thesis).
Schlatter, P., Brandt, L., de Lange, H.C., Henningson, D.S., 2008. On streak breakdown in bypass transition. Phys. Fluids 20, 101505.
Wosnik, M., Castillo, L., George, W.K., 2000. A theory for turbulent pipe and channel flows. J. Fluid Mech. 421, 115.
Wu, X.H., Moin, P., 2008. A direct numerical simulation study on the mean velocity characteristics in turbulent pipe flow. J. Fluid Mech. 608, 81.
Zaki, T.A., Durbin, P.A., 2005. Mode interaction and the bypass route to transition. J. Fluid Mech. 531, 85.